DEMISABILITY STUDY OF INDUSTRIAL TEST CASES WITH THE SPACECRAFT-ORIENTED CODE PAMPERO

M. Spel(1), J. Dumon(1), E. Constant(1), P. Van Hauwaert(1), S. Galera(2), J. Annaloro(3)

(1) RTECH, Parc Technologique Delta Sud, 09340, Verniolle, France, Email: martin.spel@rtech.fr
(2) ALTRAN SO, 4 avenue Didier Daurat, 31700 Blagnac, France (3)
(3) CNES, Centre spatial de Toulouse, 18 Avenue E. Belin, 31401 Toulouse cedex 9, France, Email: julien.annaloro@cnes.fr

ABSTRACT

CNES develops its own spacecraft-oriented tool named PAMPERO since 2013. PAMPERO aims to simulate the complete atmospheric re-entry of an entire satellite, launcher or the associated fragments due to the breakup process. One of its objectives is to provide a support to experts using current certification tools such as DEBRISK [1] in which the user must pre-fragment the space vehicle.

The purpose of this communication is to present the ability of PAMPERO [2-6] to model complex industrial test cases by analysing the surviving mass after a re-entry and the casualty area as a function of the release altitude. For each release altitude, several attitude input variations allow to evaluate the sensitivity to the release conditions. Results are compared to issue from another spacecraft-oriented tool named SCARAB [7].

1 Introduction

The French Space Operation Act (LOS) adopted on 3rd of June 2008 has established a national regime of authorization and supervision of space activities. CNES and R.Tech are since then involved in the numerical modelling of re-entering space debris. CNES is in charge of ensuring the right application of the law. To predict the debris survivability during their re-entries and assess the prospective risk on ground, the development of complete multidisciplinary tools is required.

With this in mind, CNES in collaboration with R.Tech, develops the spacecraft-oriented tool named PAMPERO since 2013. PAMPERO aims to simulate the complete atmospheric re-entry of an entire satellite, launcher or the associated fragments due to the breakup process.

The interest of developing more complex codes, such as vehicle-oriented codes, makes perfect sense. Indeed, the breakup processes are automatically computed by considering thermomechanical loads. Within the framework of the improvement/validation of PAMPERO and the in-depth understanding of the breakup process, data from experiments is essential.

The objectives of this paper are to challenge PAMPERO on an industrial test case and to present the process used in each PAMPERO simulations in order to insure a realistic interpretation of the risks on ground.

2 NUMERICAL TOOLS

2.1 PAMPERO

PAMPERO is a spacecraft-oriented code developed since 2013. Its features are as follows:

- Six degrees-of-freedom flight dynamics (2013),
- Aerodynamics and aerothermodynamics: all aerodynamics coefficients & local wall thermal heat fluxes computed (2013), [2][3][5]
- Heat transfers modelling by a 3D explicit thermal conduction module (2014) [6]
- Ablation phenomena (2015), [6]
- Mechanical stress analysis (coupling with ASTER) from the aerodynamic and thermal loads (2016/2017), [2-6]
- Multi-material objects (2017), [6]
- Fragmentation process (2017), [6]
- Simple model for damping effects (2018)
- Implicit thermal conduction model
- Aerothermodynamics for concave surfaces
- Subsonic aerodynamics

PAMPERO is currently in an important validation phase where a large number of comparisons are being performed with experiments, CFD/DSMC computations and other spacecraft-oriented tools [2-6].

2.2 GridPro

GridPro is a high-quality grid generator which permits automated multi-block structured grid generation featuring orthogonality, smoothness and robustness. GridPro is widely used in different domains like turbo machinery, Oil and Gas, Aerospace etc. . GridPro generates multiblock structured grids which are converted to unstructured hexahedral meshes.

3 Validation

A careful verification & validation process study is provided with the PAMPERO software. The strength of this procedure is that it can identify coding errors or

Proc. 8th European Conference on Space Debris (virtual), Darmstadt, Germany, 20–23 April 2021, published by the ESA Space Debris Office
Ed. T. Flohrer, S. Lemmens & F. Schmitz, (http://conference.sdo.esoc.esa.int, May 2021)

possible deficiencies of the modelling within the PAMPERO tool and in more general a vehicle-oriented code. By comparing the results computed with PAMPERO to results from the literature (mainly High-fidelity codes or experiments) we ensure realistic results or at least as accurate it can be with a vehicle-oriented approach. A continuous integration has been set up that automatically runs hundreds of tests are performed each time the code is modified in order to rapidly identify code regression.

3.1 Recent new validation cases

As an example of the validation cases, last year, two new validations of PAMPERO have been published in international journals about:

- Validation of the aerodynamic coefficients on a concave shape very challenging for simplified aerodynamics tools (concave shapes, unsteady phenomena) with CFD codes and experiments at VKI published in [5]. This publication shows how the codes based on a Modified Newton approach without any modification fail to compute the aerothermodynamic quantities on concave shapes.
- CNES has set up an experimental campaign in collaboration with TSAGI Institute (2014-2016). Study of the destruction process of Aluminium honeycomb sandwich panels (basic element of satellite structures) in the T-117 wind tunnel. In parallel, PAMPERO was challenged by the rebuilding of these destructive tests in [6].

3.2 Subsonic model validation

Hereafter is presented another validation of PAMPERO when the debris reach subsonic regimes, before the ground impact.

This aspect is very important to insure accuracy that could influence the kinetic energy and the casualty area due to the 14J limit. The accuracy of the results in the subsonic regime can change drastically the conclusions made on an industrial case.

While the Modified Newton approach gives reasonable approximations in the hypersonic flow regime on simple shapes, it is known not to be valid in the subsonic regime.

The flow in the subsonic regime is characterised by a highly complex and unsteady behaviour which cannot be captured if the flow is not modelled. The aerodynamics quantities are strongly wake dependant even for simple geometries [8][9] and a dedicated simplified model has been developed.

A development and validations have been investigated with PAMPERO at low speed regime in order to ensure a realistic assessment of the casualty area.

The validation of PAMPERO with the CFD software OpenFOAM [10] of the drag coefficient/ pressure distribution is show for a cylinder, a cube and a flat plate at low speed (Mach 0,1 and Reynolds 1e6) on the Fig.1,2,3 below for different angles of attack.

As it can be seen PAMPERO succeeds to capture the pressure distribution and thus the aerodynamic coefficients for the cube and the plate with small differences with OpenFoam. For the cylinder a good agreement is observed between CFD and PAMPERO for an angle of attack between 20 and 90. Between 0 and 20° a difference is observed due to the fact that the cylinder wake is highly complex, depending on multiple 3D perturbations in the vortex shedding which directly impact the aerodynamics as discussed in [9].

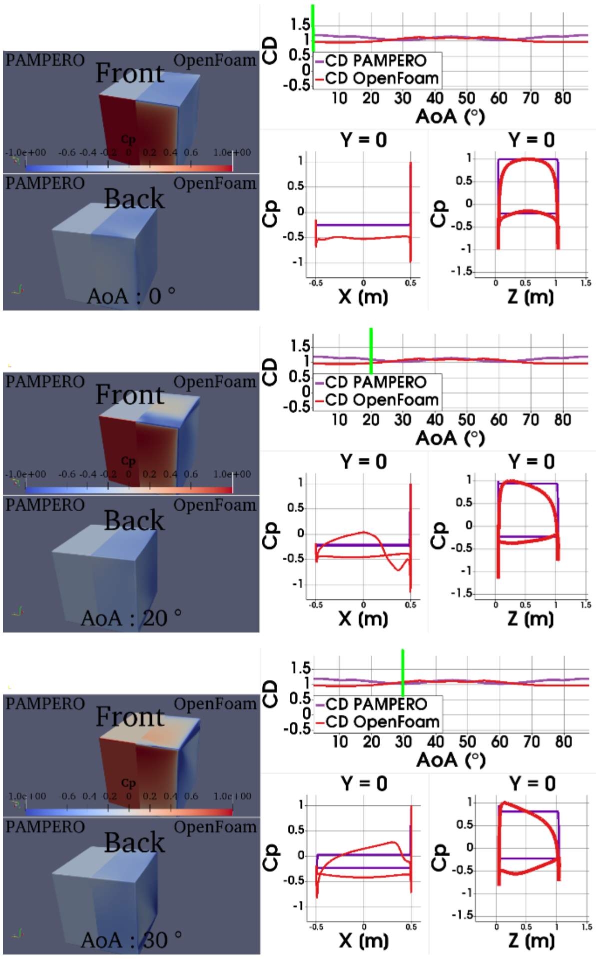

Figure 1. Cube parietal pressure, drag and pressure coefficients computed for different angles of attack with PAMPERO and OpenFOAM

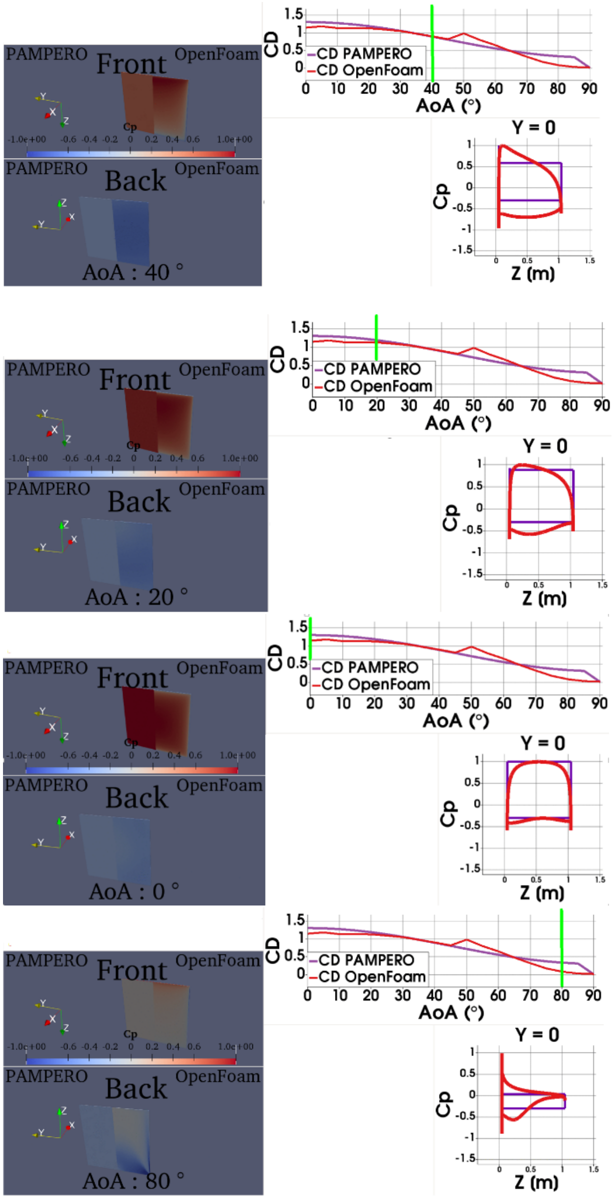

Figure 2. Flat plate parietal pressure, drag and pressure coefficients computed for different angles of attack with PAMPERO and OpenFOAM

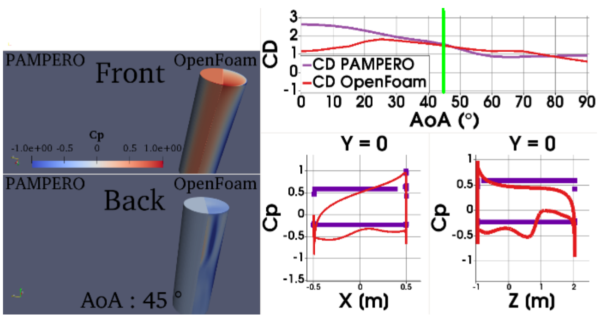

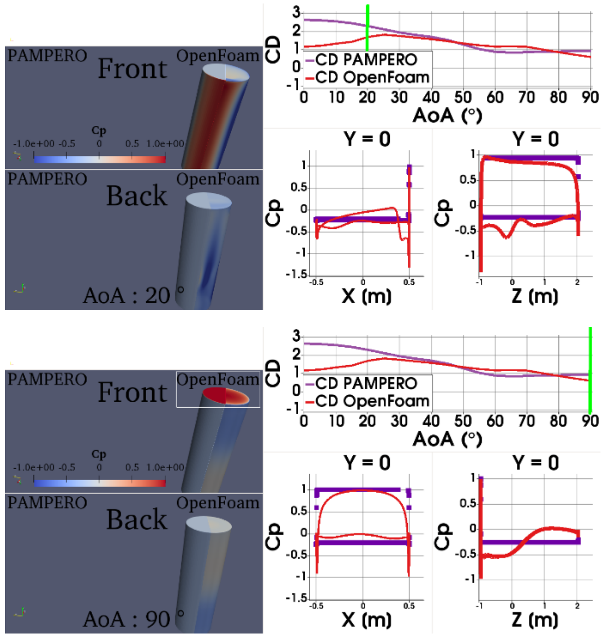

Figure 3. Cylinder parietal pressure, drag and pressure coefficients computed for different angles of attack with PAMPERO and OpenFOAM Case setup

4 Application of PAMPERO to a case study

In this section we describe the application of PAMPERO to the study of the re-entry of a reaction wheel. Since the attitude of releasee of the reaction wheel is subject to a very complex break-up modelling, in the present study we evaluate the effect of release altitude on the ground risk.

4.1 Objectives

Two objectives are foreseen in the following sections:

- Present and discuss on the results of PAMPERO on the survivability of each component of a reaction wheel
- Compare the results obtained with the ones computed by SCARAB published in [7] and discuss about the differences.

The test case will be firstly presented by an overview of the geometry used, the meshes generated and the initial orbit parameter.

4.2 Geometry

The geometry used is a Rockwell Collins RSI 68-170/60 referred to “Stainless Steel flywheel with brazed/bolted spokes” in [7] and [11] A cut view of the CAD used in the PAMPERO model is presented on Fig. 4 and the view of each component labelled from A to M with their relative position in the Reaction wheel model is presented on Fig. 5 As it can be seen from the Fig. 6 showing the mass ratio of each component over the total mass of the reaction wheel, the component D is half of the total mass of the equipment. As it is the heavier part and it is covered by the housing element (component A and C), it will be the hardest element to demise. We can induce that if this element collapses, the fragmentation will begin on the junction with the element F, as the junction on this configuration will generate high heat fluxes and mechanical loads.

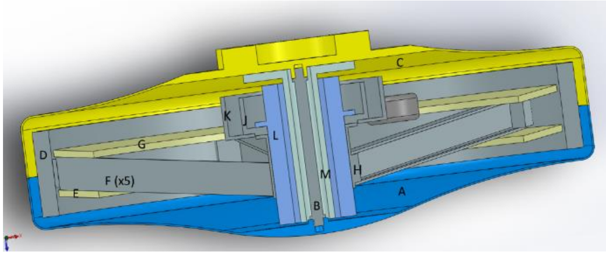

Figure 4. Rockwell and Collins Reaction wheel geometry

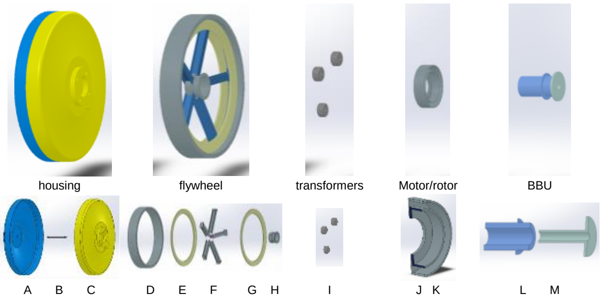

Figure 5. Rockwell and Collins Reaction wheel geometry components

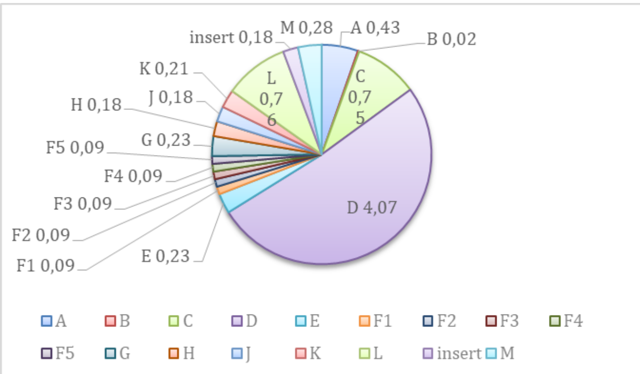

Figure 6. Rockwell and Collins Reaction wheel geometry component mass ratio

4.3 Meshes description

The GridPro software has been used to create the meshes which are constructed in a way that cells are refined close to the edges. Three level of meshes have been made in order to demonstrate a mesh convergence (Fig. 7 and Fig. 8). Without a mesh convergence study the quality of numerical results cannot be guaranteed. The results on the medium mesh approach exponentially the fine mesh results and therefore the medium mesh is kept for the rest of the study.

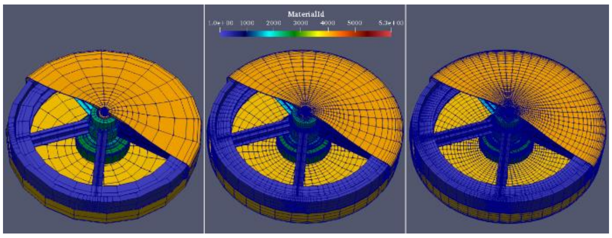

Figure 7. PAMPERO Meshes of the reaction wheel - coarse (7 303 cells), medium (59 144 cells), fine (199 611 cells)

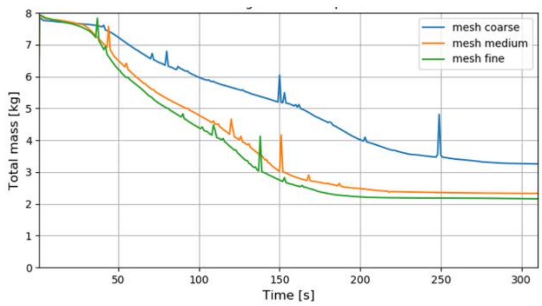

Figure 8. Mesh convergence

The results are compared to the results computed on the SCARAB mesh presented in Fig. 9.

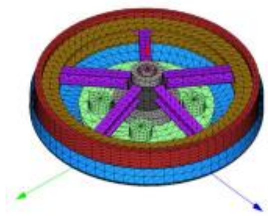

Figure 9. SCARAB Mesh

4.4 Orbital initial parameters

The initial re-entry orbit parameters, taken from [11] comes from a reference trajectory computed with DRAMA/SESAM of a sphere of 1m² cross section area and 150 kg. The trajectory computed is presented on Fig 10 and Fig 11.

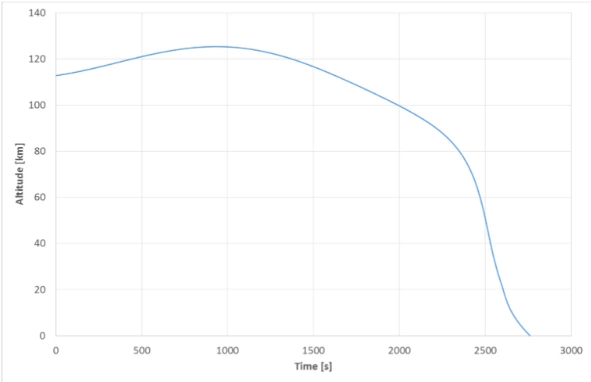

Figure 10. Initial trajectory

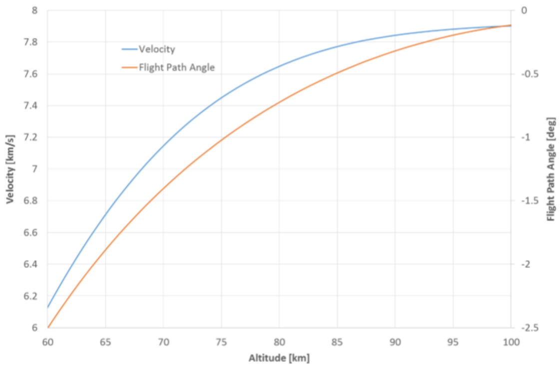

Figure 11. Initial velocity and flight path angle

From this trajectory 15 altitudes have been chosen with different initial attitudes for this study. The same matrix of 225 cases (altitudes/attitudes) computed with SCARAB [7][11] is used in this study summarized in the Tab. 1.

Table 1: sum up of the 225 test cases

5 alt x 25 attitudes	(2 x 5) alt x 10 attitude
60 km	60 +/-2 km
69 km	69 +/-2 km
78 km	78 +/-2 km
87 km	87 +/-2 km
96 km	96 +/-2 km

4.5 Results

As SCARAB and PAMPERO by default don't use the same materials properties for this study, especially for emissivity of each material, preliminary tests are presented with PAMPERO for both material databases in wind tunnel mode (constant imposed heat fluxes).

Then the results are compared on trajectories between PAMPERO with both material database (225 computations with PAMPERO database and 5 computations with SCARAB database) and the results computed by SCARAB and published in [7][11]. The differences are then discussed.

Then the probability to find each part of the reaction wheel on ground is analyzed and the fragmentation process is illustrated for one case at the highest release altitude. For the two last sections only, PAMPERO results with the PAMPERO material database is presented since PAMPERO uses a database extensively validated by many publications on experiments [12-17].

4.5.1 Material database sensitivity

PAMPERO has been run with both PAMPERO and SCARAB material database in wind tunnel mode in order to observe the impact of the different material properties on the overall degradation with a constant heat flux (taken at 500kW/m²) which is representative a heat flux seen on the atmospheric re-entry. The mass evolution for both databases is shown in Fig. 12. As it can be observed the SCARAB database results ablate the structure before the PAMPERO database. At 250 seconds of simulations we observe a difference on the survival mass about 2,5 kg. As a conclusion the differences on the two databases could then change completely the conclusions on the survival mass and the evaluation of risk on ground.

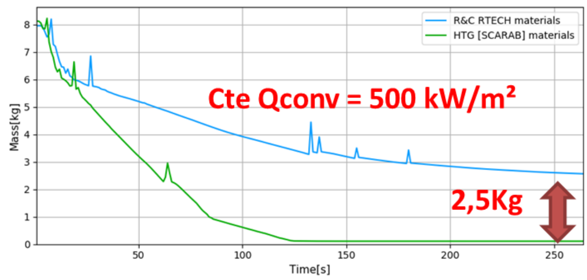

Figure 12. Comparison in Wind tunnel mode of PAMPERO with SCARAB and PAMPERO database. Evolution of mass as function of time

The Fig. 13 shows the degradation process of the reaction wheel at different times of the simulation. We can observe that already at 3 seconds the housing of the reaction wheel demises with the SCARAB material database whereas the results with PAMPERO database show that the reaction wheel is still protected by the housing. At 20 seconds the results with SCARAB database shows that the motor/rotor + BBU components already disappear whereas they just began to ablate with the PAMPERO database. We can observe that from 45 seconds up to the end of the simulation the main differences are on the degradation of the component D of the reaction wheel which is half the mass of the total reaction wheel.

a) time=3s

PAMPERO Material data's SCARAB Material data's

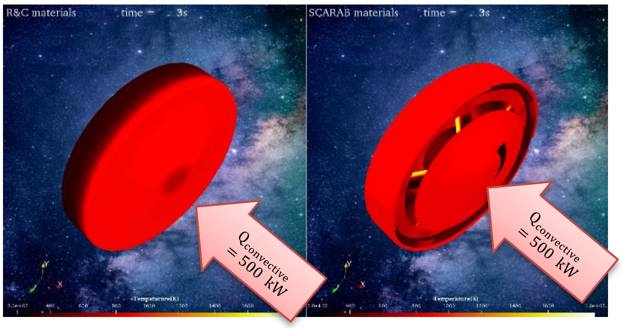

b) time=20s

PAMPERO Material data's SCARAB Material data's

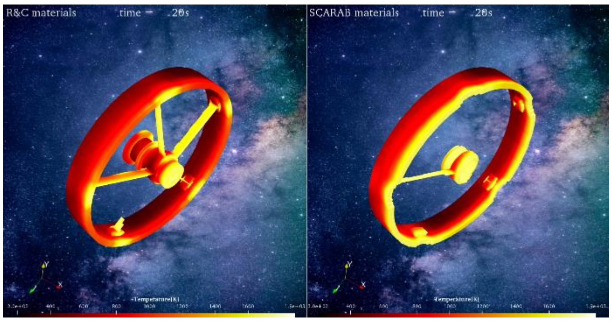

c) time=45s

PAMPERO Material data's SCARAB Material data's

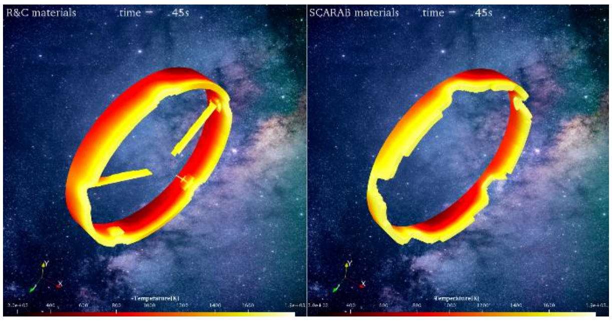

d) time=64 s

PAMPERO Material data's SCARAB Material data's

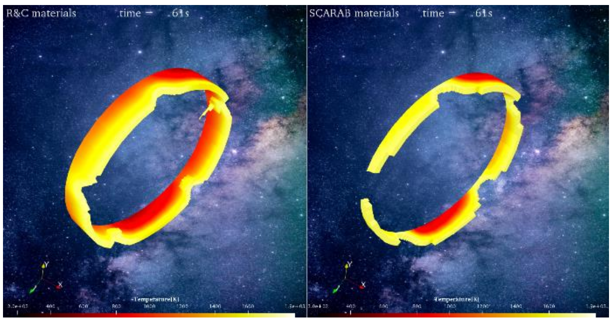

e) time=122 s

PAMPERO Material data's SCARAB Material data's

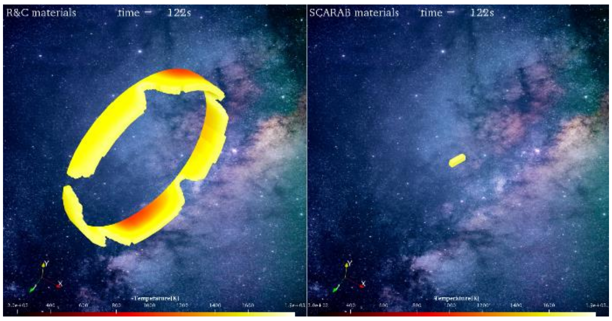

Figure 13. Comparison in Wind tunnel mode of PAMPERO with SCARAB and PAMPERO database. Evolution of the degradation as function of time

4.6 Comparisons SCARAB/PAMPERO on a trajectory

In this section we compare the results with SCARAB and PAMPERO on a full 6DOF trajectory simulation.

4.6.1 PAMPERO with PAMPERO material database versus SCARAB

When PAMPERO uses its internal material database, a huge difference on the surviving mass is observed at high altitude of release (higher than 75 km) with respect to the SCARAB results, as illustrated on Fig. 14.

As can be seen, a difference of about 2,5 kg is observed which correspond to the D component which does not completely ablate in our simulations.

Nevertheless, the curves seem to have the same inflexion point which is about 72-75 km of release altitude where the physics involved in the simulations seems to change.

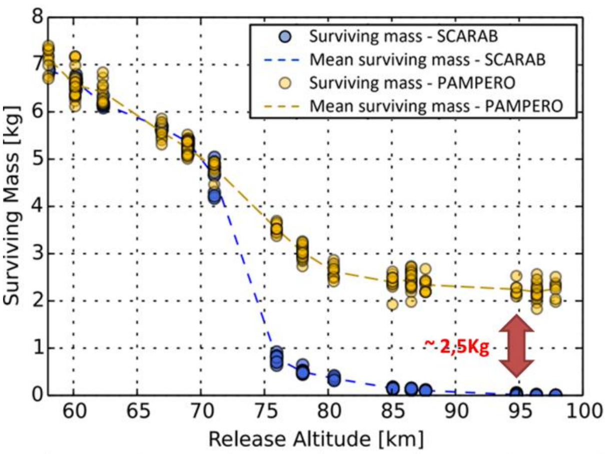

Figure 14. Comparison in trajectory mode of PAMPERO with PAMPERO database and SCARAB. Evolution of mass as function of the released altitude

These differences can also be seen on the casualty area between PAMPERO and SCARAB in the mean value found for each altitude as well as the dispersions of the results as shown on Fig. 15. A change in the casualty area can nevertheless also be observed near the inflection point at 72 km.

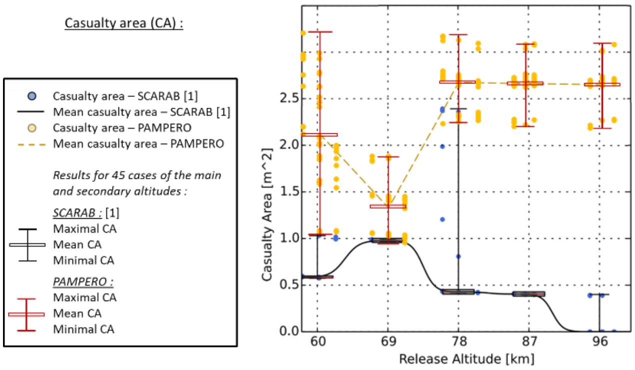

Figure 15. Comparison in trajectory mode of PAMPERO with PAMPERO database and SCARAB. Evolution of the casualty area as function of the released altitude

The huge differences found between the PAMPERO and the SCARAB results for the high release altitudes are suspected to be due to the large differences in the material database and in particular to the very low emissivity value used in the SCARAB material properties database. The emissivity values used in PAMPERO, validated on many experiments [12-17], are completely different from the ones used by SCARAB for this study.

4.6.2 PAMPERO with SCARAB material database versus SCARAB

After having identified the material properties as a potential explanation of the large differences on remaining mass, some PAMPERO simulations have been rerun with the SCARAB material properties. Due to budget and time constraints only a subset of the full matrix has been run. When PAMPERO uses the SCARAB material database, we can observe that the results are similar between the two codes as illustrated on Fig. 16.

As can be seen, only a difference remains near the inflexion point with a mass two times lower computed by PAMPERO than SCARAB at altitude of release of 69km. As only 1 case has been run, we maybe simulate an extremum value as the simulations near the inflexion point seems to be the most dispersed also with SCARAB computations.

By looking at the casualty area illustrated on Fig. 17 we can see that once again all the point computed with PAMPERO and the SCARAB database are close to the points computed by SCARAB except the point at 69km. As we can see this point have a casualty area 2 times higher than the one predicted by SCARAB, suggesting that more fragments have been created in the PAMPERO simulation. This could explain why the surviving mass is lower in PAMPERO simulation than in SCARAB one as if more fragments have been created, more surface will be exposed to the flow and the mass will be ablated more easily.

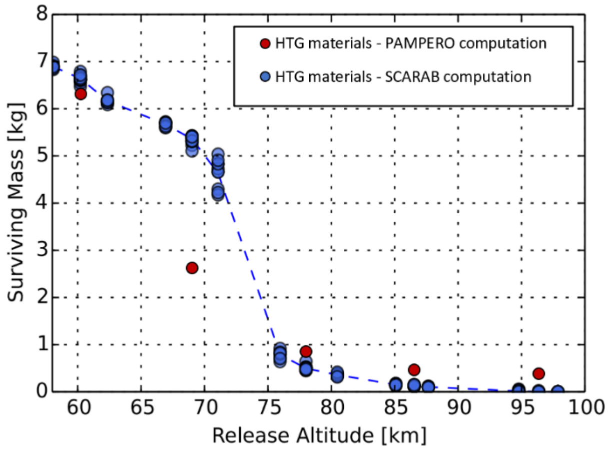

Figure 16. Comparison in trajectory mode of PAMPERO with SCARAB database and SCARAB. Evolution of mass as function of the released altitude

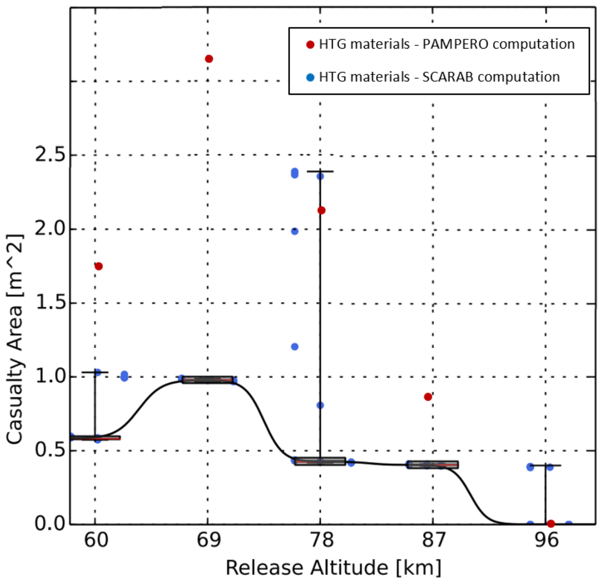

Figure 17. Comparison in trajectory mode of PAMPERO with SCARAB database and SCARAB. Evolution of the casualty area as function of the released altitude

This study shows that the huge differences comes mainly from the differences on the material properties and that when using the same material database, the results between PAMPERO and SCARAB seem to be coherent.

4.7 Fragments predicted on ground

In the rest of the study we will focus on the results obtained with the PAMPERO database.

As it can be seen on the Fig. 18 the fragment generation is split in three behaviors depending on the release altitude of the reaction wheel.

- Above 78km, where the number of fragments found on ground remains constant and way below the number of fragments generated.
- Below 71km where the number of fragments found on ground remains constant and equal to the number of fragments generated. At these altitudes of release all fragments generated will end up on the ground.
- Between 71 and 80 km corresponding almost to the range around the inflexion point mentioned in the previous section, the number of fragment found on ground is higher than the other ranges. The inflexion in the curves could then be explained by the change of dynamics in the fragment destructions.

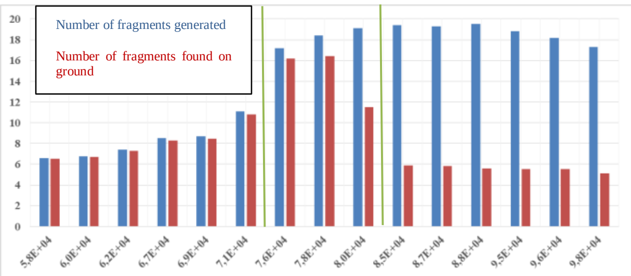

Figure 18. Number of fragments generated during the flight and number of fragments found on ground as function of the release Altitude

As illustrated on the Fig. 19 above the inflexion point only the component D, J and K are most likely to be found on ground. The component D mostly contribute to the total mass found on ground. It can reach the ground as it remains protected by the housing at the beginning of the re-entry, the equipment is then relatively protected.

At 78 km, near the inflexion point the fragment impact probability and the mean percentage of surviving mass ratio changed compare to the previous ones, showing that the dynamics of the fragment creation changes near the inflexion of the curve.

Below the inflexion point, all the components can be found on ground.

a) Altitude of release = 96 km

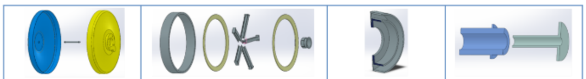

	A	B	C	D	E	F	G	H	J	K	L	M
	How many times (out of 32) these parts are found on ground ? Mean surviving mass [kg, % of initial mass] ?											
Impact probability	0	6 %	0	**100 %**	0	9 %	0	0	**81 %**	**87 %**	0	3 %
Surviving mass [kg]		$< 10^{-3}$		2,009		$< 10^{-3}$			0,087	0,141		0,009
% of initial mass		2 %		49 %		0,1 %			49 %	67 %		3 %

b) Altitude of release = 87 km

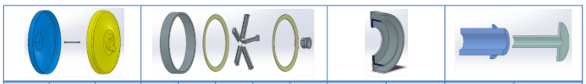

	A	B	C	D	E	F	G	H	J	K	L	M
	How many times (out of 44) these parts are found on ground ? Mean surviving mass [kg, % of initial mass] ?											
Impact probability	2 %	9 %	5 %	**100%**	0	9 %	0	5 %	**86 %**	**86 %**	0	23 %
Surviving mass [kg]	$< 10^{-3}$	0,0013	$< 10^{-3}$	2,169		$< 10^{-3}$		$< 10^{-3}$	0,095	0,161		0,020
% of initial mass	0,01 %	8 %	< 0,01 %	53 %		0,04 %		0,08 %	53%	76 %		7 %

c) Altitude of release = 78 km

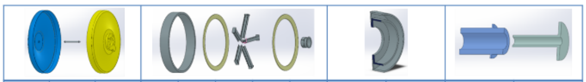

	A	B	C	D	E	F	G	H	J	K	L	M
	How many times (out of 44) these parts are found on ground ? Mean surviving mass [kg, % of initial mass] ?											
Impact probability	2 %	2 %	2 %	**100 %**	0	30 %	0	**82 %**	5 %	20 %	2 %	**86 %**
Surviving mass [kg]	$< 10^{-3}$	0,015	$< 10^{-3}$	2,893		0,005		0,053	0,055	0,083	0,003	0,054
% of initial mass	0,2 %	95 %	< 0,01 %	71 %		1 %		7 %	31 %	39 %	1 %	20 %

d) Altitude of release = 69 km

	A	B	C	D	E	F	G	H	J	K	L	M
	How many times (out of 43) these parts are found on ground ? Mean surviving mass [kg, % of initial mass] ?											
Impact probability	40 %	14 %	14 %	**100 %**	0 %	**100 %**	0 %	**100 %**	**95 %**	**93 %**	29 %	61 %
Surviving mass [kg]	0,050	0,003	0,036	4,038		0,137		0,530	0,036	0,061	0,050	0,169
% of initial mass	12 %	16 %	5 %	99 %		31 %		69 %	20 %	29 %	29 %	61 %

e) Altitude of release = 60 km

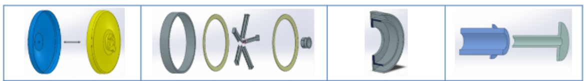

	A	B	C	D	E	F	G	H	J	K	L	M
	How many times (out of 45) these parts are found on ground ? Mean surviving mass [kg, % of initial mass] ?											
Impact probability	52 %	**100 %**	36 %	**100 %**	28 %	**100 %**	56 %	**100 %**	**100 %**	**100 %**	**100 %**	**100 %**
Surviving mass [kg]	0,128	0,015	0,188	4,075	0,185	0,197	0,192	0,759	0,179	0,204	0,172	0,275
% of initial mass	30 %	91 %	25 %	100 %	79 %	44 %	82 %	99 %	100 %	96 %	100 %	100 %

Figure 19. Probability to find each component on ground, mean surviving mass of all component and % of the initial mass of the component founded on ground for each initial altitude

As a conclusion the dynamics of fragment creation could explain the shape of the curves with an inflexion point and a change in the dynamic observed in previous sections.

4.8 Reaction Wheel flight dynamics

In this section we look in more detail on the reaction wheel demise process.

As illustrated on the Fig. 20 for a simulation at 96km of release, the reaction wheel at first begin to spin over its axis of least inertia. Then around t=25s the housing break and the interior of the reaction wheel is exposed to the flow. The component E and G rapidly break after (at about t=50s) and with ablate completely eventually. The BBU and the motor rotor starts to break into pieces around t=80s. Around t=155s the element F collapse and only the elements of the motor/rotor, the BBU and the element D remains.

The elements of the BBU ablate and only the elements J and K plus the element D which break into 5 pieces will be found on ground.

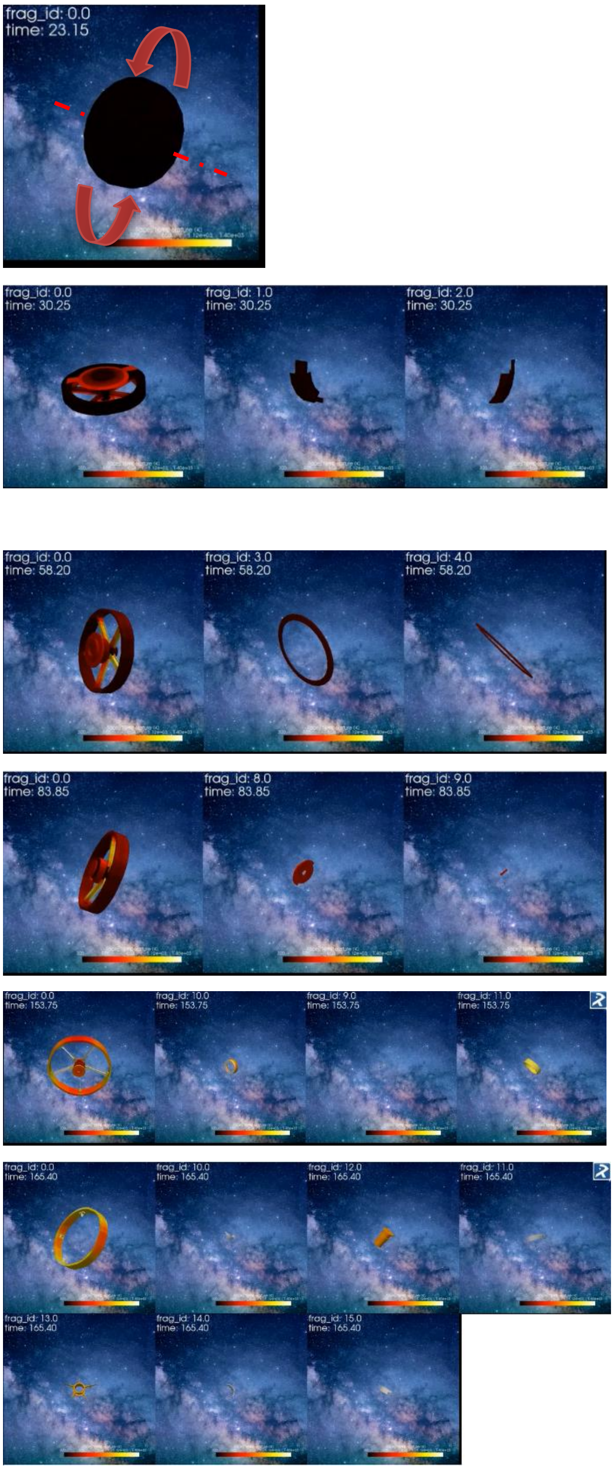

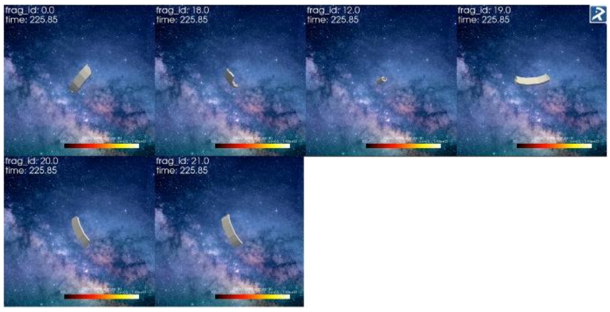

Figure 20. Reaction Wheel flight and fragmentation, PAMPERO simulation with a released altitude = 96km

5 Conclusion

As a conclusion, a study has been conducted on the reaction wheel with PAMPERO showing that several fragments with non-negligible mass are most likely to be found on the ground for several combinations of initials altitude/attitude from 60 to 96Km of release.

The study shows the existence of a key released altitude (located around 72-75km) below which all fragments generated will end up on the ground.

Since the release altitude has a major effect on the ground risk, a future study on the realistic fragmentation altitude by modelling the full satellite with the detailed reaction wheels could be achieved to evaluate more realistically the ground risk.

Important differences in the results between the PAMPERO and SCARAB code have been identified to be due in a large extend to the material properties and in particular to the emissivity values used by thee two codes, highlighting the importance of high temperature material characterization in order to reach consensus on international material databases.

Using the same material properties, the results between SCARAB and PAMPERO are satisfactory, taking into account the physical complexity of the demise process and the modelling differences in the two codes.

6 Acknowledgements

This work was carried out thanks to the financial support of the CNES.

Rockwell Collins and HTG are greatly acknowledged for their help by providing the geometry, the trajectories and the materials properties used from previous analysis.

7 References

1. Pierre Omaly, Martin Spel, DEBRISK, a tool for re-entry risk analysis, (2011), *IAASS*, Versailles

2. J. Annaloro, S. Galera, P. Kärräng, G. Prigent, T. Lips, P. Omaly, (2017), Comparison between two spacecraft-oriented tools: PAMPERO &

SCARAB, *The Journal of Space Safety Engineering*, **4**, 15–21

3. J. Annaloro, S. Galera, P. Kärräng, Y. Prévereaud, J-L. Vérant, M. Spel, P. Van Hauwaert, P. Omaly, (2017), Space debris atmospheric entry prediction with spacecraft-oriented tools, *7th European Conference on Space Debris, Darmstadt*
4. G. Prigent, J. Carro, B. Crusson, L. Stainier, (2017) First step toward fragmentation process assessment of re-entering spacecraft: mechanical stress analysis with the spacecraft-oriented simulation tool PAMPERO, *IAASS Toulouse*
5. Julien Annaloro, Stéphane Galera, Cédric Thiebaut, Martin Spel, Pierre Van Hauwaert, Guillaume Grossir, Sébastien Paris, Olivier Chazot, Pierre Omaly, (2020) Aerothermodynamics modelling of complex shapes in the DEBRISK atmospheric reentry tool: Methodology and validation, *Acta Astronautica* **171**, 388-402
6. J. Annaloro, V. Ledermann, E. Constant, M. Spel, C. Vasse, V. Rivola, S.M. Drozdov, P. Omaly, (2020) Rebuilding with PAMPERO of destructive hypersonic tests on honeycomb sandwich panels in the T-117 wind tunnel, *Journal of Space Safety Engineering*, **7**(2), 113-124
7. Patrik Kärräng, Tobias Lips, Tiago Soares, (2019), Demisability of critical spacecraft components during atmospheric re-entry, *Journal of Space Safety Engineering*, **6**(3), 181-187
8. H. Sakamoto and H. Haniu. (1990), A study on vortex shedding from spheres in a uniform flow, *ASME Digital collection,*: **386** (112)
9. C.H.K. Williamson, (1996), Vortex dynamics in the cylinder wake, *Annu. Rev. Fluid Mech*, **28,**477-539.
10. Hrvoje Jasak, (1996), Error Analysis and Estimation for the Finite Volume Method with Applications to Fluid Flows, *PhD Thesis Imperial College*
11. Geert Smert, (2017). Demisability Assessment of Reaction Wheels, *Clean Space Industrial Days*
12. M. Balat-Pichelin , J.L. Sans, E. Bêche, V. Flaudb, J. Annaloro, (2017), Oxidation and emissivity of Inconel 718 alloy as potential space debris during its atmospheric entry, *Materials Characterization*, **127**, 379–390
13. Marianne Balat-Pichelin & Barka Lucile, (2020), Behavior of TA6V Alloy at High Temperature in Air Plasma Conditions: Part 1—Oxidation *Journal of Materials Engineering and Performance*, **29**, 4597–4605
14. M. Balat-Pichelin, J. Annaloro, L. Barka & J. L. Sans, (2020), Behavior of TA6V Alloy at High Temperature in Air Plasma Conditions: Part 2—Thermal Diffusivity and Emissivity *Journal of Materials Engineering and Performance*, **29**, 4606–4616
15. L. Barka, M. Balat-Pichelin, J.-L. Sans, E. Bêche, (2019), Oxidation and emissivity of Invar 36 alloy in air plasma at high Temperatures, *Journal of Alloys and Compounds,* **772**, 1003-1016
16. M. Balat-Pichelin, A. Bousquet, (2018), Total hemispherical emissivity of sintered SiC up to 1850 K in high vacuum and in air at different pressures, *Journal of the European Ceramic Society*, **38,** 3447–3456
17. M. Balat-Pichelin, D. De Sousa Meneses, J. Annaloroc, (2019), Behavior and optical properties of Zerodur® at high temperatures, *Infrared Physics and Technology*, **101**, 68–77